Structural Health Monitoring of Wind Towers: Residual Life Estimation

M. Benedetti and V. Fontanari

Department of Materials Engineering and Industrial Technologies, University of Trento, via Mesiano 77, 38123 Trento (Italy)
matteo.benedetti@ing.unitn.it, vigilio.fontanari@ing.unitn.it

ABSTRACT. *Elastic-plastic fracture toughness and fatigue crack growth resistance of full penetration butt welds were experimentally investigated. The obtained results were used to predict the critical crack size and the time to structural collapse of weld joints typically adopted in tubular towers of windmills. For this purpose, heavy in-service loading conditions were considered. In this way, it was possible to quantify the minimum crack size that shall be detected by a structural health monitoring system, in order to maintain the structure within a reasonable time interval.*

INTRODUCTION

The strong drive to harness wind energy has recently led to the consideration of new installation sites for wind turbines, including mountain regions [1]. In comparison with conventional sites, such locations are more critical, because the more severe weather and wind conditions. A major concern for wind farm installation in these sites is related to the reliability of the supporting structures in the life-long period. It is common practice that slender vertical structures exposed to wind, like chimneys or flexible steel towers, may experience large vibrations and repeated stress cycles leading to fatigue cracking [2]. For instance, recent failures of lighting towers have raised questions about the robustness and safety of the existing inventory of similar structures [3]. Failure analyses attested small cracks initiation along the weld toe of the fillet weld joining the pole to the shoe base and their propagation, due to wind-induced cyclic loads, through the wall thickness and around nearly 80% of its circumference before catastrophic failure.

Although the Eurocode 1 [4] recently codified the first method to take it into account in the design of structures exposed to wind actions, the strength prediction of wind towers is difficult. First, because cracks can initiate at different points, including the base flange-to-column weld, the handhold detail and the anchor rods [2,3]. Second, the response depends on the complex interaction between wind action and dynamic vibration. Third, the response of the wind tower to wind actions is made even more complicated by the fact that the nacelle atop the tower rotates in order to keep the rotor aligned with the wind direction.

Recently, the authors explored the possibility of employing suitable strain sensors to reveal the onset of fatigue cracks [5]. For this purpose, the perturbation of the strain field in the vicinity of a crack located in a critical site for the structural integrity of an existing wind tower was numerically assessed. Typical heavy in-service loading conditions were estimated, starting from the dynamic characterization of the wind tower in terms of Eigen-frequencies and damping ratios as well as from nacelle acceleration spectra. Several strategies for crack detection were investigated, taking into account the possibility of wind direction changes and/or wind calm phases. They are based on a radial arrangement of strain sensors around the tower periphery in the vicinity of the base weld joint. The most promising strategy uses the strain difference between adjacent strain sensors as an index of the presence of a crack.

The present paper is aimed at investigating possible strategies for residual fatigue life assessment and management once the crack has been detected. For this purpose, fracture mechanics tests have been carried out using welded samples to quantify the resistance to fatigue crack growth as well as the elastic-plastic fracture toughness of weld joint at the tower base. These material strength characteristics have been incorporated into a frequency domain method to predict the residual life of the tower. In this way, it is possible to identify inspection-maintenance intervals, within them the structure can safely operate.

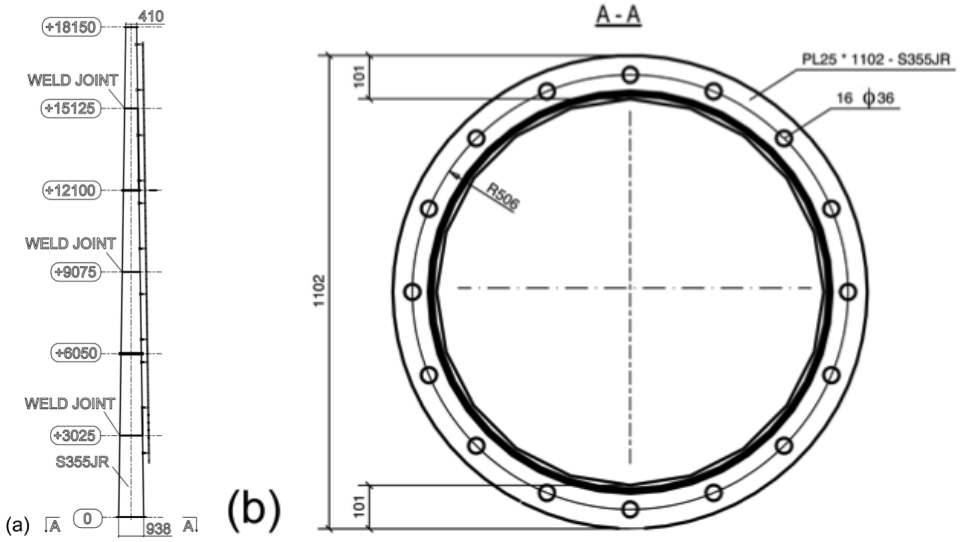

Figure 1. Technical drawing of the wind tower investigated in this study. (a) Overview and (b) detail of the base flange.

BACKGROUND

The Wind Tower and the Aerodynamic Actions

The two-bladed, teeter hub, downwind, free yawing, stall controlled GAIA wind turbine described in [5] has been chosen to explore the possibility of remote structural health

monitoring. The truncated conical (mean diameter: 0.55 m at the top to 1.10 m at the base, 18.1 m height) tubular tower, made of hot-dip-galvanised S355JR steel, is shown in Fig. 1a. The shell thickness is 6 mm. The tower is composed of three sections that are connected to each other by means of double flanges with fully preloaded bolts. A similar configuration has been used at the joint between the top flange and the yaw ring. The bottom flange (depicted in Fig. 1b) has been fixed at the foundation by partially prestressed anchors arranged in a circle on the outer side of the shell. This type of joint is particularly prone to fatigue damage because of the flexibility of the flange. Therefore, in order to meet the strict requirements of the fatigue design, the shell is connected to the flanges with full penetration high quality butt welds. More details thereof will be given in the following.

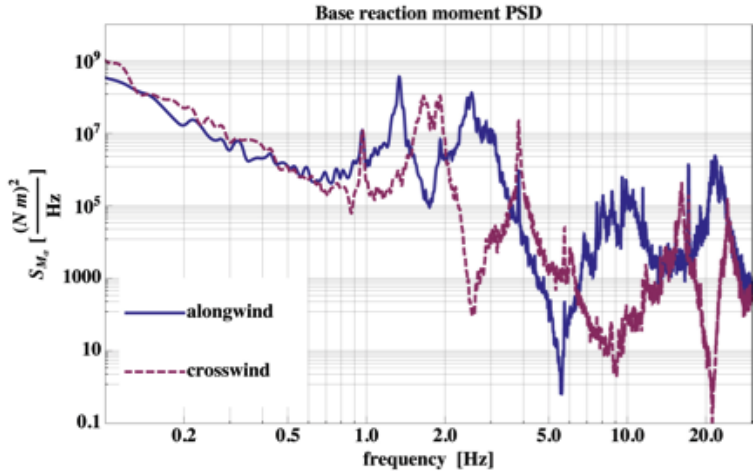

Figure 2. Power spectral density (PSD) of the base reaction moment due to longitudinal and lateral turbulence.

An experimental campaign was carried out in [5] in order to investigate the dynamic behaviour of the wind tower in terms of Eigen-frequencies, damping behaviour and in-service loading spectra. Specifically, a modal identification of the structure was performed by positioning six accelerometers along the tower and inducing impulse excitation using an instrumented shock hammer. The frequency response function (FRF) has been calculated in order to extract Eigen-frequencies and damping ratios of the structure. The dynamic loads acting on the wind tower during the in-service conditions were estimated by instrumenting the turbine nacelle with three piezo-electric accelerometers. Since the wind turbine is free yawing so as to align the rotor with the wind direction, the three linear acceleration components were measured alongwind (x -axis), crosswind (y-axis) and upward along-gravity (z-axis). The static alongwind action has been computed using the aerodynamic and structural parameters of the windmill. Conversely, the fluctuating buffeting actions have been indirectly calculated starting from the longitudinal and lateral acceleration spectra. For this purpose, a dynamic Finite Element (FE) model of the wind tower has been set up to compute the transfer functions

from turbulence to the corresponding nacelle acceleration component and from turbulence to the corresponding base reaction moment component. Figure 2 illustrates the Power Spectral Density (PSD) of the base reaction moment due to longitudinal and lateral turbulence. The maximum amplitude of the fluctuating base reaction moment, which is expected from the PSD shown in Fig. 2, has been calculated using the so-called $\pm 3\sigma$ criterion [6]. Hence, a maximum amplitude of 77.1 kN m and 58.9 kN m is obtained due to alongwind and crosswind loads, respectively, while a far smaller static alongwind base reaction moment equal to 5.8 kN m is predicted. Finally, the alongwind base reaction moment equal to 38.7 kN m, corresponding to a cumulative occurrence probability of 10% that this reference value is exceeded, has been used as a representative value for in-service loading conditions.

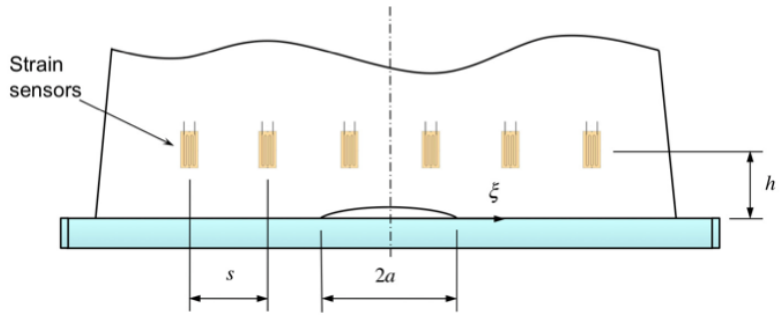

Figure 3. Schematic illustration of a circumferential through crack propagating along the weld toe of the base flange. A radial arrangement of axial strain sensors is shown.

Crack Detection Strategy using Strain Sensors

Predicting the fatigue damage caused by the time-varying wind actions is quite cumbersome for many reasons, among them the uncertainty about wind loading, wind directionality, fatigue crack initiation sites, and the effect of complex geometric details like weld junctions. Therefore, a safe running of the wind turbine could take advantage of a reliable non-destructive damage detection (NDD), giving the basis of any decision to repair, rehabilitate, or replace the structure. Usually, in structures like supporting masts or lighting poles, critical sites for fatigue crack initiation and propagation are located at the welds between rings and tube [3]. In [5], a radial arrangement of strain sensors around the tower periphery in the vicinity of the base weld joint, schematically shown in Fig. 3, has been considered to reveal the perturbation of the strain field caused by the onset of fatigue cracks. It has been found that the most promising strategy uses the strain difference between adjacent strain sensors as an index of the presence of a crack. Accordingly, the presence of a crack produces a strain gradient much more pronounced than that observed in the undamaged portion of the structure. Therefore, if the strain variation between adjacent sensors significantly deviates from the strain gradient measured by the remaining sensors, the likelihood that a crack has initiated in the structure is very high. Such an approach requires that at least one sensor is located above the crack face, where the strain is released by the presence of the defect. In principle, this requirement is met if the sensor spacing pitch s (see Fig. 3) is shorter than

the crack length 2*a*. So, for any disposition of the sensors, at least one sensor is placed in the zone where the strain release is more pronounced. In [5], it has been demonstrated that strain sensors usually employed for structural monitoring of civil constructions [7] have sufficient accuracy to detect cracks with half-length down to 20 mm.

In conclusion, the major limiting factor for fatigue crack detection is the number of strain sensors, depending on the budget allocated for the health monitoring of the structure, rather than the strain sensor sensitivity. The minimum detectable crack size shall be chosen on the basis of other considerations, like the compatibility between the residual service-life after damage detection and the inspection/maintenance schedule of the structure. Specifically, the residual service-life depends on (i) the extreme wind conditions expected for the wind turbine, (ii) typical in-service wind loading and directionality, (iii) fracture toughness, and (iv) fatigue crack growth resistance of the material. The latter two issues will be analysed in the following.

EXPERIMENTAL MATERIAL AND PROCEDURES

Base Metal, Welding and Fracture Mechanics Specimens

The experimentation was performed on the construction steel S355JR, used for the tubular tower, supplied in the form of 15 mm thick rolled plate. Monotonic tensile tests (initial strain rate of $1x10^{-3}$ s^{-1}) were performed in the longitudinal (L) orientation using plane hourglass specimens. The results, summarized in Table 1, show a yield stress higher than 355 MPa, combined with a high ductility (total elongation of 30%).

Table 1. Mechanical properties of the base material

Material	Yield stress (MPa)	Ultimate stress (MPa)	Total elongation (%)
S355JR	380	560	30

Weld joints have been fabricated by butting together two pieces of the original plate, which were previously chamfered to form a double V-groove that helps compensating for warping forces. Before welding, the two pieces were kept in place with an appropriate fixture to minimize the joint misalignment. The full penetration double welded butt joints were executed according to the same indications followed for the wind tower. Specifically, the metal-arc active gas (MAG), semi-automatic welding process was applied with the active shielding gas Ar+10%CO_2 and the wire EN 440-G42 4M G3Si1, whose mechanical properties declared by the supplier are: yield stress 420 MPa, ultimate tensile stress 500 MPa, total elongation 22%. Therefore, the strength mismatch factor, defined as the ratio between the weld metal and the base metal yield strength, is equal to 1.11, thus indicating about 10% over-matching.

The fracture mechanics tests were carried out on compact C(T) specimens whose geometry, according to the standard ASTM E1820-09, is illustrated in Fig. 4a. They were extracted from both the virgin and the welded plates, as schematically shown in

Fig. 4b, in order to introduce the fatigue crack starter notch (1) inside the Base Material (BM), (2) in the Weld Metal (WM) centre, (3) in the Heat Affected Zone (HAZ) along the weld bead. After machining, the specimens were grinded and polished to facilitate the monitoring of the crack advance.

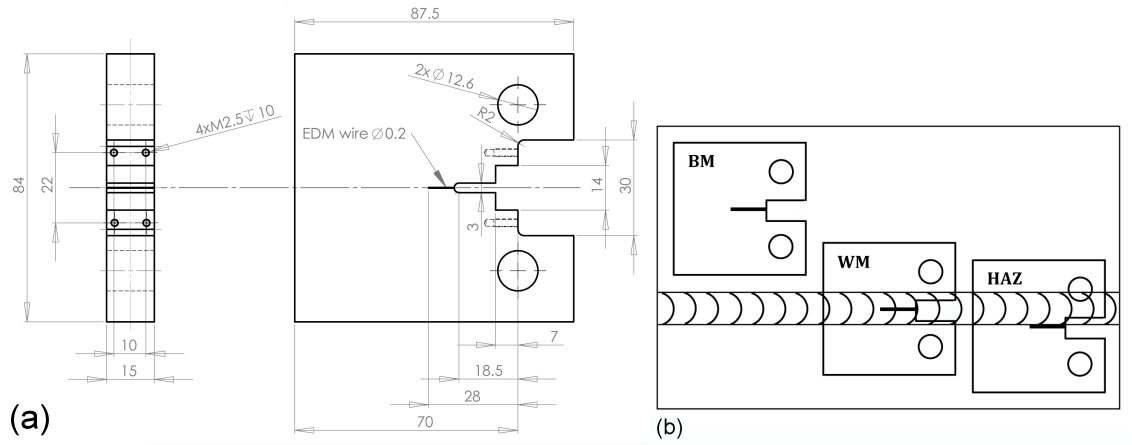

Figure 4. (a) Geometry of C(T) specimens used in this study. (b) Extraction scheme from the welded plates.

Fatigue Crack Growth Testing

The fatigue crack growth testing was performed according to the standard ASTM E647-08. The experiments were conducted in the laboratory environment on a servo-hydraulic testing machine. A sinusoidal pulsating (load ratio R = 0.1) load waveform was applied at a frequency of 30 Hz. During fatigue testing, optical microscopy (travelling microscope) was used for crack length monitoring.

Fracture Toughness (J-Integral) Testing

The fracture toughness testing was performed according to the standard ASTM E1820-09. The specimens were fatigue pre-cracked in the laboratory environment using a resonant testing machine with load ratio R = 0.1 keeping the maximum stress intensity factor less than 24 MPa$\sqrt{\text{m}}$. The initial crack length to specimen width ratio (a/W) was about 0.45. Subsequently, to enforce the plane strain condition, 20% side grooves were introduced, resulting in a net thickness (B_N) of 12 mm. The single specimen method was adopted to determine the J-resistance curve J_R. The crack opening displacement was recorded by a CMOD clip gauge during constant displacement rate (0.5 mm/min – under displacement gauge control). The crack length was measured by the compliance technique and verified by post-test optical crack size measurements. For this purpose, in order to minimize the effect of load relaxation on the compliance measurements, causing a time-dependent nonlinearity in the unloading slope, the specimen was held at a constant CMOD for 1 min dwell time up to force stabilization prior to initiating the unloading.

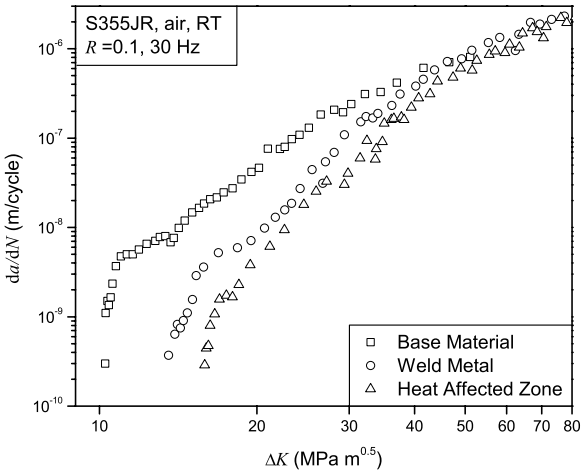

Figure 5. Fatigue crack growth curves.

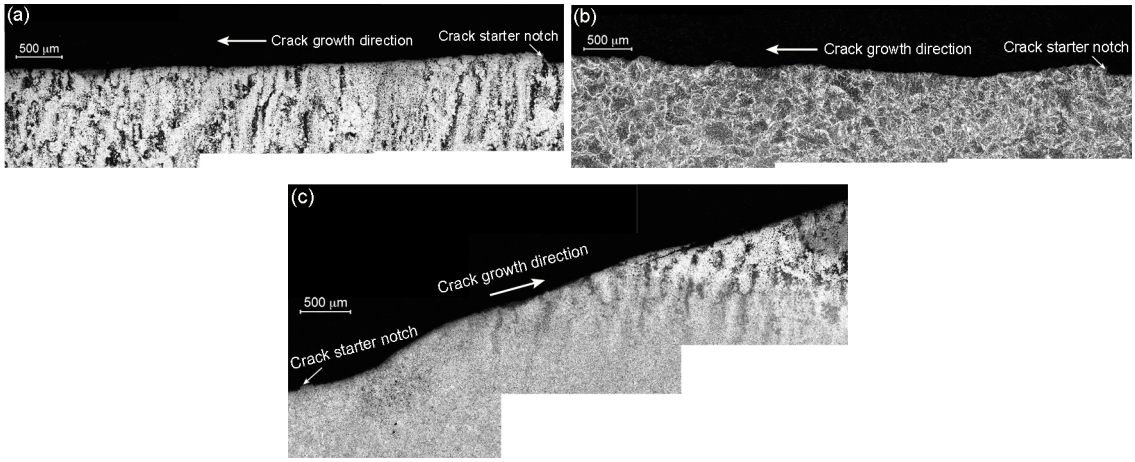

Figure 6. Fatigue crack paths. (a) Base Material, (b) Weld Metal, (c) Heat Affected Zone.

EXPERIMENTAL RESULTS

Fatigue Crack Growth Curves

The fatigue crack growth curves are shown in Fig. 5. It can be noted that both WM and HAZ exhibit slower crack growth rates as compared to BM, especially in the near-threshold regime. This can be reasonably imputed to surface residual stresses, introduced by the welding process both in WM and HAZ (as attested by blind-hole-drilling measurements, here not reported for the sake of brevity), responsible for crack closure and crack growth retardation. In addition, crack growth rates are even slower in

HAZ than in WM. A possible explanation thereof can be given by the analysis of the fatigue crack paths illustrated in Fig. 6a-c, for BM, WM, and HAZ, respectively. While crack propagation in BM and WM occurs on a plane approximately orthogonal to the loading direction, crack advance in HAZ occurs along an inclined direction, which is unfavourably oriented with respect to the stress axis. Apparently, the cracks initiated in the HAZ spontaneously tend to propagate outside the HAZ towards the BM.

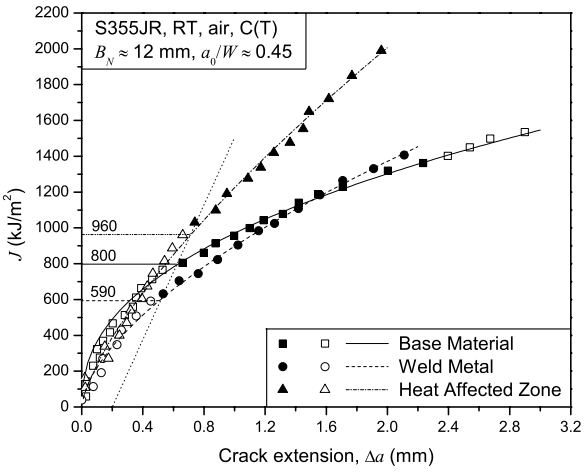

Figure 7. *J*-resistance curves.

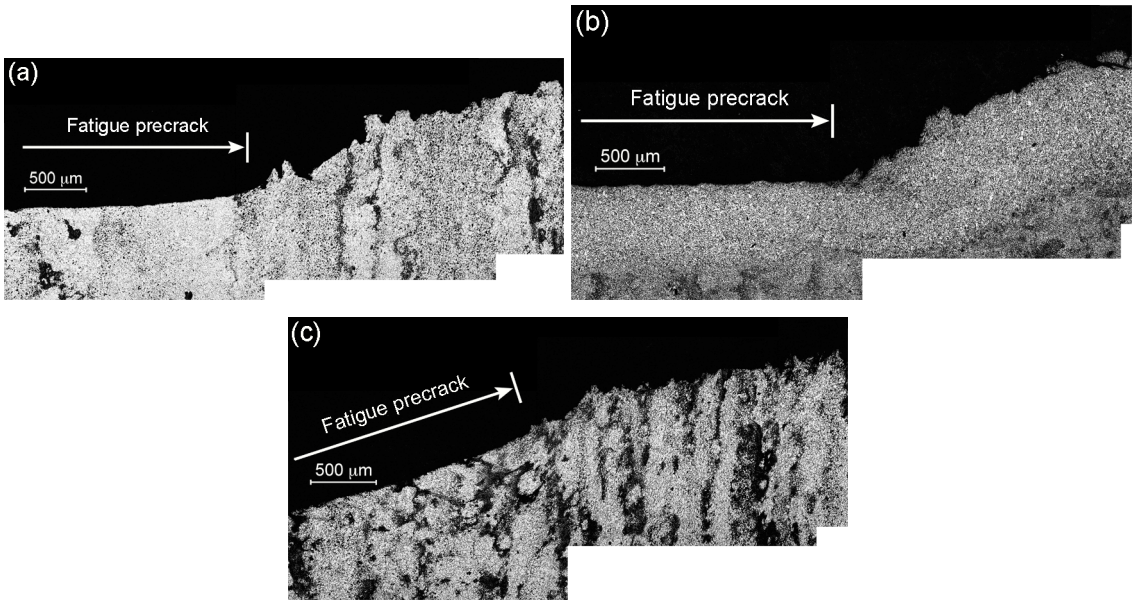

Figure 8. Fracture crack paths. (a) Base Material, (b) Weld Metal, (c) Heat Affected Zone.

J-Resistance curves

The J_R curves are shown in Fig. 7. Significant stable tearing crack extension was observed for all tested specimens. In particular, the WM specimen exhibits the lowest fracture toughness. To this regard, it should be mentioned that only the test on the WM condition ended with a plane-strain fracture toughness value J_{Ic}, while BM and HAZ samples yielded a thickness-dependent fracture toughness. Notably, the HAZ condition shows the highest J_c value. This can be explained by analysing the crack paths illustrated in Fig. 8a-c, for BM, WM, and HAZ, respectively. As expected, the fatigue precrack in BM and WM samples is orthogonal to the stress axis, while fatigue crack growth in HAZ occurred along an inclined plane due to the preferential propagation outside the HAZ. However, during the final monotonic loading, the crack path is rather dictated by the side grooves that have been machined after fatigue precracking. In this way, stable tearing crack extension is forced along a material-unfavourable crack path, resulting in higher *J*-resistance curve.

RESIDUAL LIFE OF THE WIND TOWER

The residual life of the wind tower, after the strain sensor has detected fatigue crack initiation, depends on both (i) the speed of the subsequent crack propagation and (ii) the size of the critical defect that can be tolerated by the structure during wind gust loading. In order to determine these two parameters, it will be assumed that the crack path will lie on the weld toe of the base flange. This seems reasonable in consideration of the crack paths observed in Figs. 6 and 8, the stress amplification caused by the circumferential constraint opposed by the rings, and the stress concentration effect exerted by the weld toe. In addition, for a worst-case analysis, the fatigue crack growth resistance properties of the BM will be used. In fact, the residual stress field caused by the weld treatment and likely responsible for fatigue crack growth retardation strongly depends on the structure geometry, mainly the thickness of the welded parts, which significantly differs from that of the C(T) specimens used in the present work.

Critical Defect Size

The elastic-plastic fracture analysis of circumferential through-wall-cracked wind tower subjected to gust wind loading was carried out with the commercial code Ansys ® Rel. 11 using the same FE model illustrated in [5]. In particular, the weld joint was assumed to restore the structural continuity of the component. The weld toe profile was modeled as a 135°-opening angle sharp notch. Furthermore, the elastic-plastic properties of the steel, determined through monotonic tensile tests, were implemented in the model. The rate-independent, incremental theory of plasticity has been used for the FE calculations. In particular, the plasticity theory uses the von Mises yield surface model with associated plastic flow rule. The hardening rule used is that of multilinear kinematic hardening. *J* was computed according to the contour integral method.

The wind loading was simulated through a concentrated force applied to the tower upper extremity, so that the point of maximum bending stress coincides with the crack

centre. The magnitude of the concentrated force was chosen to yield the same maximum reaction moment estimated in [5] according to the ±3σ criterion. For a worst-case analysis, along- and crosswind actions were assumed to be in phase and then vectorially summed. Wind actions were assumed to scale with the square of the wind mean speed, thus under the realistic hypothesis that turbulence is linearly proportional to the wind mean speed.

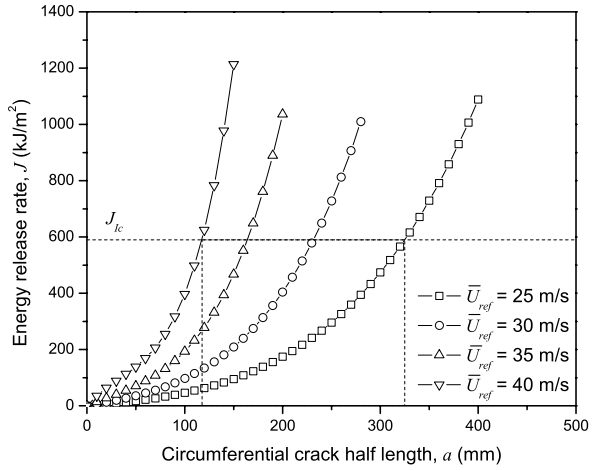

Figure 9. Energy release rate J as a function of the crack length a.

Figure 9 depicts the applied energy release rate J plotted as a function of the crack length a and compared with the plane strain fracture toughness J_{Ic} of the WM. The curves are parametric in the reference velocity $\bar{U}_{ref}$, i.e. the mean wind velocity at 10 m height, in open country. Its values have been chosen as those that may occur under extreme weather conditions in high-altitude alpine environment [8]. The adopted conservative failure criterion is based on the onset of stable crack growth, which occurs when:

$$J\left(a_c, \bar{U}_{ref}\right) = J_{Ic} \tag{1}$$

It can be noted that in the explored reference velocity interval, the critical circumferential crack half-length ranges from about 120 to 325 mm.

Fatigue Crack Growth and Maintenance Intervals

Once the strain sensors have detected a defect along the weld toe, a given number of fatigue cycles is required to bring the crack size to its critical value a_c before structural collapse. In the present paper, we propose to use the frequency domain method developed by Zuccarello and Adragna [9] to estimate the expected crack growth rate under wide band random loading, directly form the PSD of the base reaction moments

shown in Fig. 2. The expected time to crack growth from the initial detected length a_0 to the critical length a_c is expressed by:

$$\bar{T}(a_0,a_c)=\frac{2\pi\sqrt{\lambda_2/\lambda_4}}{C\sigma_X^{n-1}}\int_{a_0}^{a_c}\left(Y\sqrt{\pi a}\right)^{1-n}\left[\frac{(h_1)^{\frac{1}{3}(2n-7)}}{(h_2)^{\frac{2}{3}(n-2)}}+\frac{1}{9}\left(\frac{(h_3)^{\frac{1}{3}(2n-7)}}{(h_4)^{\frac{2}{3}(n-2)}}-\frac{(h_1)^{\frac{1}{3}(2n-7)}}{(h_2)^{\frac{2}{3}(n-2)}}\right)\left(\frac{K_c}{3\sigma_X Y\sqrt{\pi a}}-1\right)\right]\mathrm{d}a$$

$$h_i=h_i(\alpha_X,\beta_X)$$

$$\alpha_X=\frac{\lambda_2}{\sqrt{\lambda_0\lambda_4}}\quad\beta_X=\frac{\lambda_1}{\sqrt{\lambda_0\lambda_2}}\quad\sigma_X=\sqrt{\lambda_0}$$

$$\lambda_i=2\int_0^{+\infty}\omega^i S_X(\omega)\mathrm{d}\omega \tag{2}$$

where C, n, K_c are materials constant involved in the Forman crack propagation law and determined through non-linear fitting of the Paris curve plotted in Fig. 5, σ_X is the standard deviation of the random stress process, h_i (i=1,…,4) are stochastic mean functions of the irregularity factor α_X and wide band parameter β_X, which in turn depend on the i-order spectral moment of the random stress process, and Y is the crack shape-factor computed in [5].

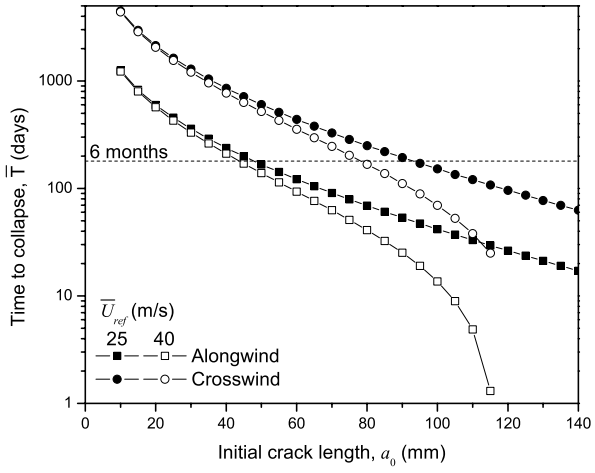

Figure 10. Time to structural collapse as a function of the initial detected crack length.

It has been assumed that the wind direction is approximately constant during the integration interval. This is consistent with anemometric investigations of the site where the turbine is installed which attest preferential NNW-SSE wind direction and diurnal excursions in the blowing orientation. Since the fluctuating (zero-mean) wind actions are preponderant with respect with the static alongwind loading, the change in wind orientation is expected not to significantly affect the estimations made using Eq. (2). Obviously, this model does not take into account the occurrence of wind gusts during wind turbine operation. However, the present approach is deemed conservative because

overloads will result in crack growth retardation. Along- and crosswind loading were considered separately in Eq. (2) so as to get an upper and a lower bound of the time $\bar{T}(a_0, a_c)$. The time to structural collapse $\bar{T}$ is plotted in Fig. 10 as a function of the initial detected crack length a_0. The curves are parametric in the reference velocity $\bar{U}_{ref}$. Initial crack lengths larger than 140 mm have not been considered, since in [5] it was demonstrated that simpler crack detection techniques, for instance based on natural frequency changes, can be adopted. Considering that maintenance of wind towers located in high-altitude alpine environment might be impossible for 6 months during the winter season, the requested minimum detected crack size ranges from 40 to 90 mm, depending on the expected wind loading conditions, this means that the tower shall be instrumented with a radial arrangement of strain sensors varying from 50 to 22, as schematically illustrated in Fig. 3.

CONCLUSIONS

Elastic-plastic fracture toughness and fatigue crack growth resistance of full penetration butt welds were experimentally investigated. The obtained results were used to predict the critical crack size and the time to structural collapse of weld joints typically adopted in tubular towers of windmills. For this purpose, heavy in-service loading conditions were considered. In this way, it was possible to quantify the minimum crack size that shall be detected by a structural health monitoring system, in order to maintain the structure within a reasonable time interval.

REFERENCES

1. Battisti, L., Giovannelli, A. (2006) *ASME ESDA 2006-8th Biennial ASME Conf. on Engineering Systems Design and Analysis (Turin).*
2. Robertson, A.P., Hoxey, R.P., Short, J.L., Burges, L.R., Smith, B.W., Ko, R.H.Y. (2001) *Wind Struct.* **4**, 163–76.
3. Dexter, R.J., Ricker, M.J. (2002) *Fatigue-resistant design of cantilevered signal, sign, and light supports NCHRP Report* 469 (Washington, DC: Transportation Research Board, National Research Council).
4. European Committee for Standardization (CEN) (1994) Basis of design and actions on structures *Eurocode 1, Part 2-4: Wind actions. ENV 1991-2-4 (Brussels)*.
5. Benedetti, M., Fontanari, V., Zonta, D. (2011) *Smart Materials and Structures* **20**, 055009.
6. Tunna, J.M. (1985) *Proc. Inst. Mech. Eng.* **199,** 249–57.
7. Majumder, M., Gangopadhyay, T.K., Chakraborty, A.K., Dasgupta K., Bhattacharya D.K. (2008) *Sensors Actuators A* **147**, 150-64.
8. Goyette, S. (2008) *Nat. Hazards* **44**, 329-39.
9. Zuccarello, B., Adragna N.F. (2007) *Int. J. Fatigue* **29**, 1065-79.